Biosurface and Biotribology

WILEY

The Institution of Engineering and Technology

ORIGINAL RESEARCH OPEN ACCESS

Facile Preparation of 3D Aerogels With Aligned Fibre Structure for Filtration Application

Chunmei Feng | Xingyu Zhang | Yuchen Zhou | Wenyan Zhang | Botao Song

Key Laboratory of Synthetic and Natural Functional Molecule of the Ministry of Education, College of Chemistry and Materials Science, Northwest University, Xi'an, Shaanxi, China

Correspondence: Botao Song (botaosong@nwu.edu.cn) | Wenyan Zhang (zhangwy@nwu.edu.cn)

Received: 29 July 2025 | **Revised:** 18 February 2026 | **Accepted:** 21 March 2026

Keywords: 3D aerogel | aligned structure | bioinspired | filtration

ABSTRACT

3D fibre aerogels with aligned architecture, due to their high porosity, interconnected pore structure and high specific surface area, show great potential in sound absorption, oil-water separation and air filtration. Herein, we present a novel and simple long straight bundle electrospinning strategy inspired by *Darwin's bark spider* to prepare 3D aligned fibre aerogels. Different from the conventional electrospinning, whipping instability of the fibre is effectively eliminated by manipulating the distribution of electric field lines during the long straight bundle electrospinning, resulting in the formation of a 3D aligned fibre aerogel. The detailed long straight bundle electrospinning process (formation of fibre bundle, flying path of fibre bundle and deposition of fibre bundle) along with the underlying mechanism are systematically studied. Based on this theoretical basis, scalable fabrication of the 3D flexible aligned fibre aerogel with an ultrahigh fibre alignment degree of 0.93 and an ultrathick structure (2.8 cm) is achieved in one step. As a proof of concept, we investigate the use of the 3D aligned fibre aerogel in air filtration. It is found that the fibre aerogel shows excellent $PM_{1.0}$ and $PM_{2.5}$ filtration performance in both perpendicular to and parallel to fibre alignment direction. Interestingly, the pressure drop in the direction parallel to fibre alignment is only 21 Pa, which is much lower than that in the direction perpendicular to fibre alignment. We also compare the filtration performance of our 3D fibre aerogel with other filters and find that the comprehensive performance of our aerogel is obviously better.

1 | Introduction

3D fibre aerogel assembled by lots of ultrafine fibres is a new kind of aerogel. This novel aerogel integrated the merits of both conventional aerogels and ultrafine fibres, including high porosity, low density, interconnected pores and also high specific surface area, leading to their vast application scenarios, such as air filtration, oil-water separation, sound absorption, tissue regeneration and heat insulation [1–4]. Numerous effects have been devoted to preparing 3D fibre aerogels. Among these, template-assisted collection [5], self-assembly [6], 3D printing [7], gas foaming [8] and freeze-drying [9] are the most commonly used methods. For instance, Cao et al. first split the nanocrystal bundles from cellulose nanocrystals powders and prepared a polyacrylonitrile nanofiber membrane by electrospinning. Then, the fibre aerogel was prepared by a freeze-drying technique and further heat-treated to obtain cross-linked fibre aerogel [10]. Similarly, Zhu et al. extracted cellulose nanofibers (CNF) from a northern bleached softwood kraft pulp as the 3D printing ink and then prepared CNF aerogel using the 3D printing technique. The CNF aerogel was further modified for fast solar-driven atmospheric water harvesting [11]. Jin et al. synthesised graphene oxide (GO) using the Hummers method and prepared polyacrylonitrile/itaconic acid fibre membrane by electrospinning. Then, the 3D fibre aerogel was successfully fabricated by the combination of gas foaming, freeze drying and coating with GO [12]. As mentioned above, these preparation methods involved expensive setups and suffered from multistep processes, which greatly hindered the large scale production, and were also widely used [13].

Recent studies indicated that the aligned fibre structure is beneficial to improve materials properties [14–17]. For instance, Li et al. prepared a silicon nitride sponge containing highly aligned fibres, and the sponge demonstrated a high air filtration efficiency of over 99.8% and a low pressure drop of only 131 Pa. The filtration performance with the aligned structure was superior to that with the random fibre structure [18]. Zhu et al. developed an anisotropic wood aerogel with high fibre alignment. The aerogel exhibited excellent oil absorption capacity [19]. Panatdasirisuk et al. designed a polycaprolactone nanofiber membrane for separating oil-in-water emulsion. By stretching to align the internal fibres, the aligned fibre membrane was able to exclude oil from the ultra-small diameter (< 18 nm) oil-in-water emulsion droplets and maintained a high volumetric flux of 70 $L \cdot m^{-2} h^{-1} bar^{-1}$ [20]. For example, Vaquette et al. developed a new technique involving braiding and electrospinning to prepare aligned poly (L-lactic acid-ε-caprolactone) electrospun microfibers for ligament tissue engineering. The composite scaffold exhibited an elastic modulus (150 ± 14 MPa) similar to the modulus of human ligaments owing to the aligned structure. Biological evaluation results showed that cells could spontaneously align along the direction of microfiber alignment compared with random scaffolds [21]. Based on these, the aligned fibre structure may be important for high-performance fibre aerogels and thus it is of great significance to propose a simple and versatile method to prepare 3D fibre aerogels with high fibre alignment.

Nature offers a plethora of excellent design that inspires valuable insights into the preparation of new materials. In the nature, *Darwin's bark spider*, a notable example of a predator, is capable of spitting out a long and highly aggregated bundle of silk over 20 m for its prey. The spitting aligned fibre bundle of *Darwin's bark spider* inspired us to propose a long straight bundle electrospinning strategy to fabricate a 3D aligned fibre aerogel. Unlike the conventional single-jet spinning process, the biggest difference of the new spinning strategy was that, after finely controlling the electric field, an aligned fibre bundle was ejected from the Taylor cone and the bundle was then flown straight, resulting in an ultra-thick bioinspired 3D aligned fibre aerogel. We systematically investigated the straight bundle spinning process (formation of fibre bundle, flying path of fibre bundle and also fibre deposition) and the mechanism behind 3D aerogel formation. Furthermore, bioinspired 3D aligned fibre aerogel was prepared, and the fibre alignment was analysed by combining scanning electron microscopy (SEM) and a two-dimensional fast Fourier transform (FFT) approach. Finally, as a proof of concept, we investigated the potential of the bioinspired 3D aligned fibre aerogel in particulate matter filtration, and anisotropic air filtration performance (parallel and perpendicular to the fibre alignment direction) was carefully evaluated.

2 | Materials and Methods

2.1 | Materials

PS (M_w: 350000 g/mol, ρ: 1.04 g/mL) was purchased from Sigma-Aldrich Company. Anhydrous lithium chloride (LiCl) was obtained from Tianjin Tianda Chemical Reagent Factory. Silver nitrate ($AgNO_3$) was supplied by Tianjin Tiangan Chemical Technology Development Co. Ltd. Anhydrous calcium chloride ($CaCl_2$) was supplied by Tianjin Sheng'ao Chemical Reagent Co. Ltd. N, N-Dimethylformamide (DMF) and tetrahydrofuran (THF) were provided by Shanghai Aladdin Reagent Co. Ltd. All reagents and solvents were used as received without further purification.

2.2 | Fabrication of the Bioinspired 3D Aligned Fibre Aerogels

A homogeneous solution containing LiCl was obtained by adding 75 mg LiCl powders into a mixed solvent containing 2 mL of DMF and 2 mL of THF. The mixture was stirred for 30 min at room temperature. Then, 0.75 g PS particles were added to the above solution. Subsequently, the solution was placed on an electrospinning device. The spinning voltage was controlled at 13 kV. The distance between the nozzle and the rotated drum was 8 cm, and the flow rate was maintained at 1.5 mL/h. The speed of rotation of the collector was set to 50 rpm. To investigate the effect of salt species on the long straight bundle electrospinning process, the other two salts, $CaCl_2$ and $AgNO_3$, were also added into the solution for spinning, respectively.

To study the influence of salt concentration on the long straight bundle electrospinning process, a solution with different concentration of LiCl (2.5%, 5%, and 10%) was prepared. Firstly, 18.75, 37.5 and 75 mg of LiCl powders were added to a mixed solvent of 2 mL of DMF and 2 mL of THF. Then, 0.75 g PS particles were added to the solution. The mixture was stirred at room temperature for 12 h. The spinning parameters were consistent with that mentioned before. Finally, the fabricated bioinspired 3D aligned fibre aerogels were vacuum-dried at 50°C for 24 h to remove the residual solvent.

A 2D PS fibre membrane was also prepared as control. A homogeneous PS spinning solution was obtained by adding 0.75 g PS particles into a mixture of 2 mL of DMF and 2 mL of THF. The fibre membrane was deposited on aluminium foil under a high-voltage power supply of 8 kV. The flow rate was 1.0 mL/h, and the spinning distance was 15 cm. Finally, the fabricated 2D PS fibre membrane was vacuum-dried at 50°C for 24 h to remove the residual solvent.

2.3 | Characterisation

The morphology of the prepared bioinspired aerogel was characterised using SEM (SU8010, Hitachi). The thickness of the aerogel was measured with a thickness gauge. The mechanical properties were tested both parallel and perpendicular to the fibre alignment directions using a tensile testing machine (sunszy-2000, utm2103, Shenzhen, Suns). The conductivity tester (DDS-308F) was utilised to measure the conductivity of the spinning solutions at room temperature. Additionally, the viscosity of the spinning solutions at room temperature was tested using a rotational digital viscometer (HS YZL-H). Three tests were conducted for each solution and the results were averaged to minimise errors. The volume density (ρ) of the aerogel was calculated using Equation (1):

$$\rho = M/V \quad (1)$$

where V is the volume of the bioinspired nanofiber aerogel and M is its mass.

An FFT analysis of the SEM image was performed to determine the fibre alignment in aerogels. The FFT output images were generated by using a module in the software ImageJ, which contained greyscale pixel patterns that reflects the degree of fibre alignment in the SEM image. The aerogel alignment degree (S) was also determined by the following Equation (2):

$$S = \left(3\cos^2\theta - 1\right)/2 \quad (2)$$

where θ was the angle between the direction of the long axis of each individual fibre and the drum rotation direction.

2.4 | Anisotropic Filtration Performance of the Bioinspired 3D Aligned Fibre Aerogels

The TSI 8532 automated filtration tester was utilised to assess the filtration performance of the bioinspired 3D aligned fibre aerogels in the directions parallel to and perpendicular to fibre alignment. The number of parallel replicates was at least three for each experiment. The instrument was linked to a particle generator capable of producing particles ranging in diameter from 0.3 to 10.0 μm. A fan connected to the particle generator facilitated driving the generated aerosol particles through the filters. Aerosol wind speed was measured using an anemometer (FMA1002R-V1, OMEGA). Two automated filtration testers were employed for measuring aerosol concentrations before and after passing through the filters. Additionally, the pressure drop across the filter was gauged utilising a pressure transducer (DP-CLCTM5825). Particulate aerosol tests were conducted at room temperature with a fixed aerosol wind speed of 0.20 km/h, and the filtration efficiency (η) of the filters was calculated using Equation (3):

$$\eta = [(N_1 - N_2)/N_1] \times 100\% \quad (3)$$

where N_1 and N_2 are the particle concentrations upstream and downstream of the filter, respectively. The pressure drop ΔP (the difference in pressure before and after filtration) is calculated as follows Equation (4):

$$\Delta P = P_2 - P_1 \quad (4)$$

where P_1 and P_2 are the pressures before and after filtration, respectively.

The quality factor (QF) was a crucial parameter for evaluating the filtration performance of filters and could be calculated as follows Equation (5):

$$\mathrm{QF} = -\ln(1 - \eta)/\Delta P \quad (5)$$

3 | Results and Discussion

3.1 | Characterisation of the Bioinspired 3D Aligned Fibre Aerogel

The *Darwin bark spider* possesses elongated major ampullate ducts. Through the precise modulation of the spinning environment, it produces dragline silk exhibiting ultrahigh toughness and exceptional tensile strength. Due to this outstanding toughness, the silk can be aerially transported by wind currents to span river gaps for effective insect capture. Inspired by the spitting of the long fibre bundle phenomenon of *Darwin bark spider*, a novel long straight bundle electrospinning technique was proposed to fabricate bioinspired 3D aligned fibre aerogel (Figure 1a). During spinning, a fine and narrow bundle was observed to fly to the rotated drum, highly similar to the spider spitting phenomenon, as shown in Figure 1b. The fibre bundle was then wrapped on a rotated drum to form a thick 3D aligned fibre aerogel. Figure 1c revealed that the thickness of the bioinspired aerogel increased with spinning time, and the thickness could increase to 2.8 cm after 6 h of deposition. As depicted in Figure 1d, the fibre aerogel showed an ultralow density about 3.88 mg/cm^3 and could freely stand on the top of a flower, indicating its ultra-light feature. The bioinspired aerogel also exhibited good tensile strength and could bear a weight 1000 times heavier than itself without breaking (Figure 1e). In addition to mechanical robustness, it also displayed good mechanical flexibility. It could be knotted and even repeatedly twisted without destruction (Figure 1f,g).

The SEM images in Figure 1h,i indicated that fibres in the bioinspired aerogel were highly aligned along the drum rotation direction, and the fibre surface was smooth without beads. Furthermore, the alignment degree of the fibres in the bioinspired aerogel was further investigated by the FFT method. From Figure 1j, it was found that the FFT output image displayed a linear pattern, indicating that the fibres showed good alignment. The degree of alignment S was calculated to be high up to 0.93, further indicating high alignment of the fibres, as shown in Figure 1k.

3.2 | Effect of LiCl Concentration on the Formation of the Bioinspired Aligned Fibre Aerogels

The effect of LiCl concentration on fibre flying path, deposition width and fibre alignment of the resultant fibre materials was thoroughly studied. As shown in Figure 2a1–a5, for the electrospinning of the pristine PS solution, the fibres underwent a strong whipping motion with the deposition width over 20 cm, and a 2D membrane was finally obtained after continuing fibre deposition. When the loading ratio of LiCl increased to 2.5%, an obvious whipping phenomenon was also observed, resulting in the formation of the 2D fibre membrane (Figure 2b1). Interestingly, the whipping of the fibre was effectively hindered when the loading ratio was fixed at 5% (Figure 2c1). Besides, we also observed that the deposition width of the fibres was obviously shortened, and the thickness of the membrane was significantly improved. During the electrospinning of PS/10%LiCl solution, a

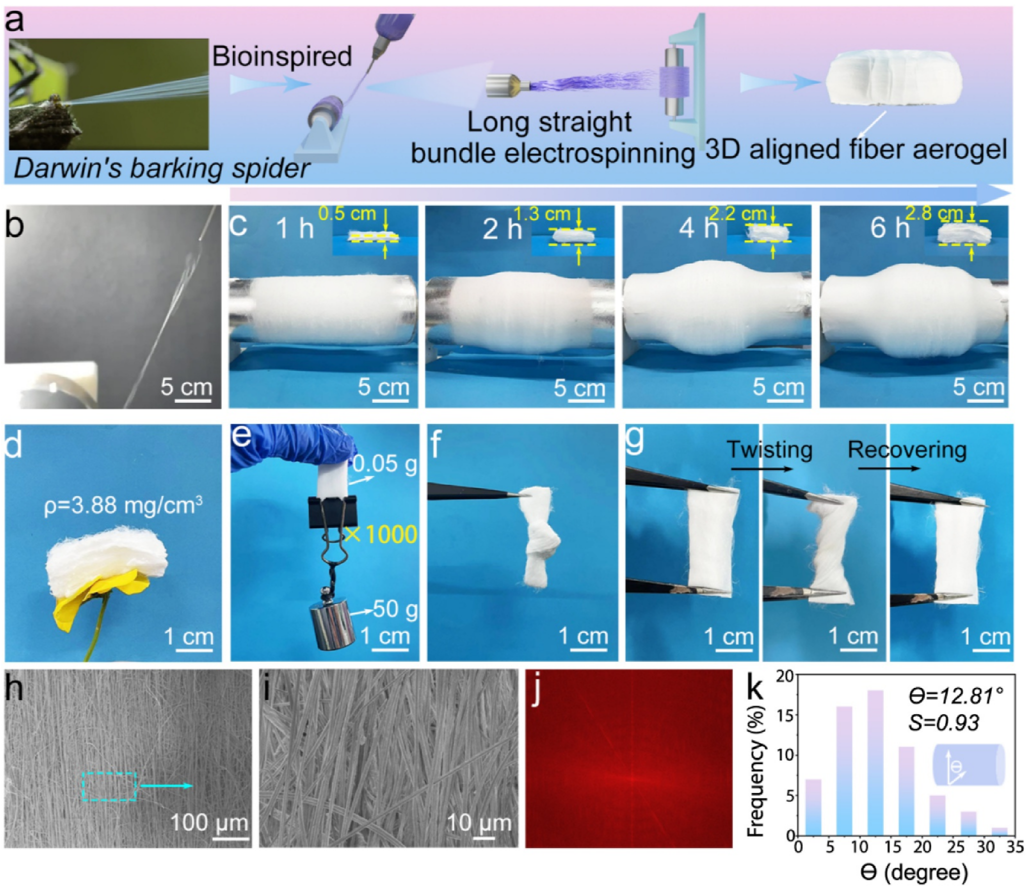

FIGURE 1 | (a) Schematic illustration of the bioinspired concept and the preparation of the 3D aligned fibre aerogel. (b) Digital photograph of the straight fibre bundle and the novel spinning process. (c) Thickness variation with the increasing spinning time. (d) Ultra-lightness of the aerogel. (e–g) The aerogel is mechanically robust. (h) Low magnification and (i) high magnification of the aligned fibres. (j) FFT result, (k) alignment degree of the fibres.

long straight fibre bundle could be observed, and a thick fibre aerogel was found to be deposited on the drum (Figure 2d1,d2). The deposition width of the fibre aerogel was gradually decreased to only 10 cm, which was much narrower than that of the obtained 2D membrane (Figure 2b2,c2,e). The SEM results in Figure 2b3–d3 revealed a gradual increase of fibres alignment with different LiCl concentrations. Meanwhile, the FFT output images and the quantitative result of the alignment degree S also proved that the fibres in the 3D aerogel showed a highly aligned structure (Figure 2b4–d4,b5–d5). In order to clarify the underlying mechanism, both the conductivity and viscosity of the four spinning solutions were tested. The results in Figure 2f displayed that the conductivity of the four spinning solutions exhibited a notable increase from 0.46 to 820 μS/cm, whereas the corresponding viscosity did not undergo a significant change with the increasing LiCl concentration.

3.3 | Effect of Salt Species on the Formation of the Bioinspired Aligned Fibre Aerogels

We carefully studied the effect of three different salts, namely $AgNO_3$, $CaCl_2$ and LiCl, on the fibre motion path. As shown in Figure 3a1–c1, all the three kinds of fibre bundles underwent a straight path, and no obvious bundle whipping could be observed. The widths of the fibre bundles for the PS/10%$AgNO_3$ aerogel, PS/10%$CaCl_2$ aerogel and PS/10%LiCl aerogel were 1.5, 2.5 and 0.5 cm, respectively. Interestingly, different from the 2D membrane obtained from the conventional electrospinning, we observed that the resultant PS/10%$AgNO_3$ aerogel, PS/10%$CaCl_2$ aerogel and PS/10%LiCl aerogel all showed a 3D thick architecture, as shown in Figure 3a2–c2. In addition, we also observed that the deposition of the fibre was focused at the centre of the drum, and the deposition widths of these aerogels were very narrow (Figure 3d).

We then employed the SEM technique to observe the morphology of these fibre aerogels and found that most of the fibres were in a parallel direction (Figure 3a3–c3). The FFT output images in Figure 3a4–c4 indicated a linear pattern for the three kinds of aerogels, suggesting that the fibres were aligned along the drum rotation direction. The average angle θ between the long axis direction of each fibre and the drum rotation direction for PS/10%$AgNO_3$ aerogel, PS/10%$CaCl_2$ aerogel and PS/10%LiCl aerogel was 16.16°, 16.25° and 13.22°, respectively. The alignment degree S was calculated to be 0.72, 0.61 and 0.92, respectively, as shown in Figure 3a5–c5. As shown in Figure 3e, we measured the conductivity and viscosity of the PS/10%$AgNO_3$, PS/10%$CaCl_2$ and PS/10%LiCl spinning solutions and found the conductivities of the solution were 310, 190 and 820 μS/cm, respectively. The viscosities of the three spinning solutions was 702, 710 and 720 cP, respectively. There was a

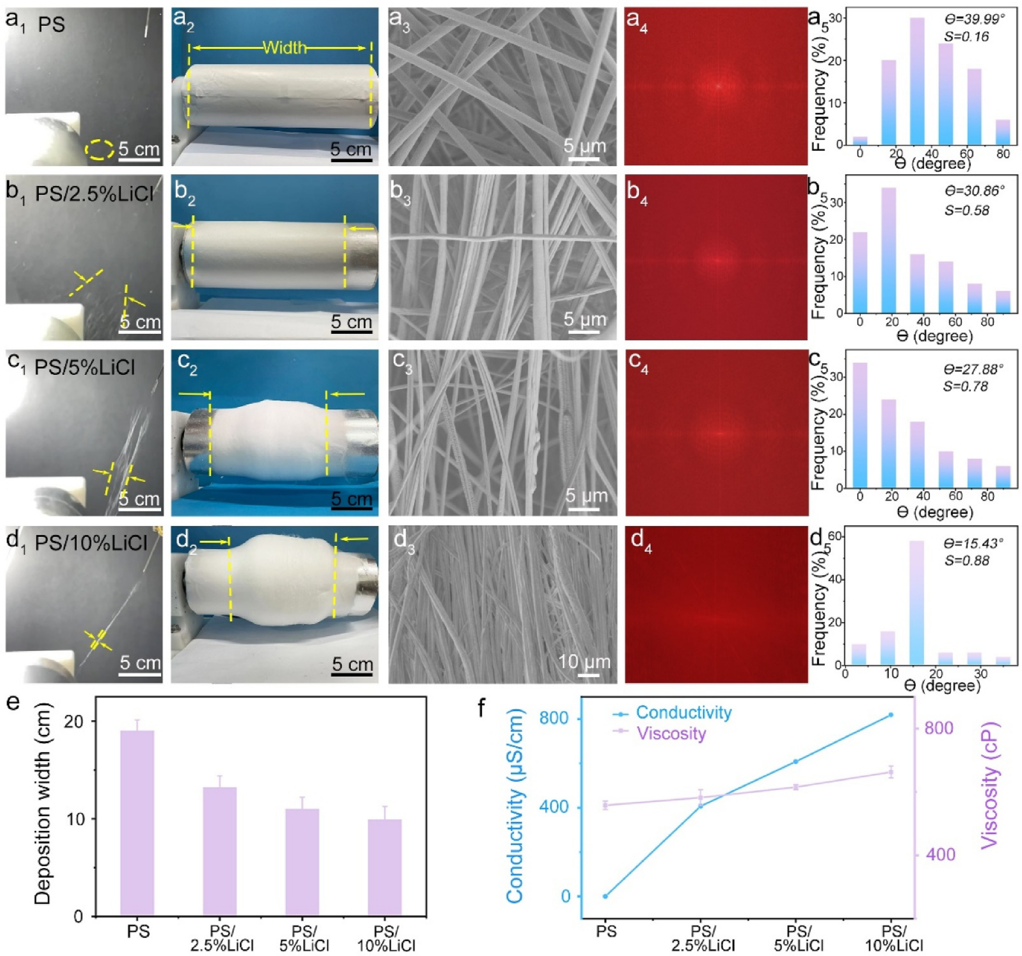

FIGURE 2 | (a_1, a_2) Whipping motion of the fibre during the electrospinning of pristine PS solution and appearance of the thin 2D PS fibre membrane. (a_3–a_5) SEM image, FFT result and fibre alignment degree S of the resultant PS fibre membrane. (b_1, b_2) Whipping motion of the fibre during the electrospinning of PS/2.5%LiCl solution and the obtained fibre membrane. (b_3–b_5) SEM image, FFT result and fibre alignment degree S of the PS/2.5%LiCl fibre membrane. (c_1, c_2) Slightly whipping motion of the fibre during the electrospinning of the PS/5%LiCl solution and appearance of the PS/5%LiCl fibre aerogel. (c_3–c_5) SEM image, FFT result and fibre alignment degree S of the PS/5%LiCl fibre aerogel. (d_1, d_2) Long straight bundle formation during the electrospinning of the PS/10%LiCl solution and appearance of the PS/10%LiCl fibre aerogel. (d_3–d_5) SEM image, FFT result and fibre alignment degree S of the PS/10%LiCl fibre aerogel. (e) Deposition widths of the four kinds of fibre materials. (f) Conductivity and viscosity of the spinning solutions with different LiCl concentrations.

significant difference in the conductivity of the three spinning solutions. On the contrary, the viscosity of the three spinning solutions remained almost unchanged for the three types of salt.

3.4 | Formation Mechanism of the Bioinspired 3D Aligned Fibre Aerogels

Generally, electrospinning is recognised to be a simple and versatile method to produce fibres. During the conventional electrospinning process, a single fibre was ejected from the charged droplet due to the low conductivity of the spinning solution. The flying fibre became highly unstable under the downward electric field force F_E and the repulsive force (F_R, $F_{R'}$), and then underwent a strong whipping motion. After the solvent evaporation, the fibres were randomly deposited on the drum in a large area with the form of the 2D membrane (Figure 4a) [22, 23].

In this study, different from the conventional electrospinning, we proposed a novel long straight bundle electrospinning strategy for the preparation of 3D aligned fibre aerogels. The possible mechanism was shown in Figure 4b. Due to the high conductivity of the spinning solution, lots of fibres were simultaneously ejected from the charged droplet. The aligned fibre bundle flew in the shortest straight path in order to immediately release large quantities of electric charge in the fibres due to the instability. Once in contact with the drum, the rotated drum will pull the aligned fibres along the drum rotation direction, and the charges could be immediately released on the conductive drum. Although when the deposition time increased, the flying fibres would deposit onto the pre-deposited fibres rather than the conductive drum. As the pre-deposited fibres were insulating, the pre-deposited fibres with massive positive charges would repel the flying fibres with like charges. Thus, a 3D fluffy aerogel with aligned fibres was formed.

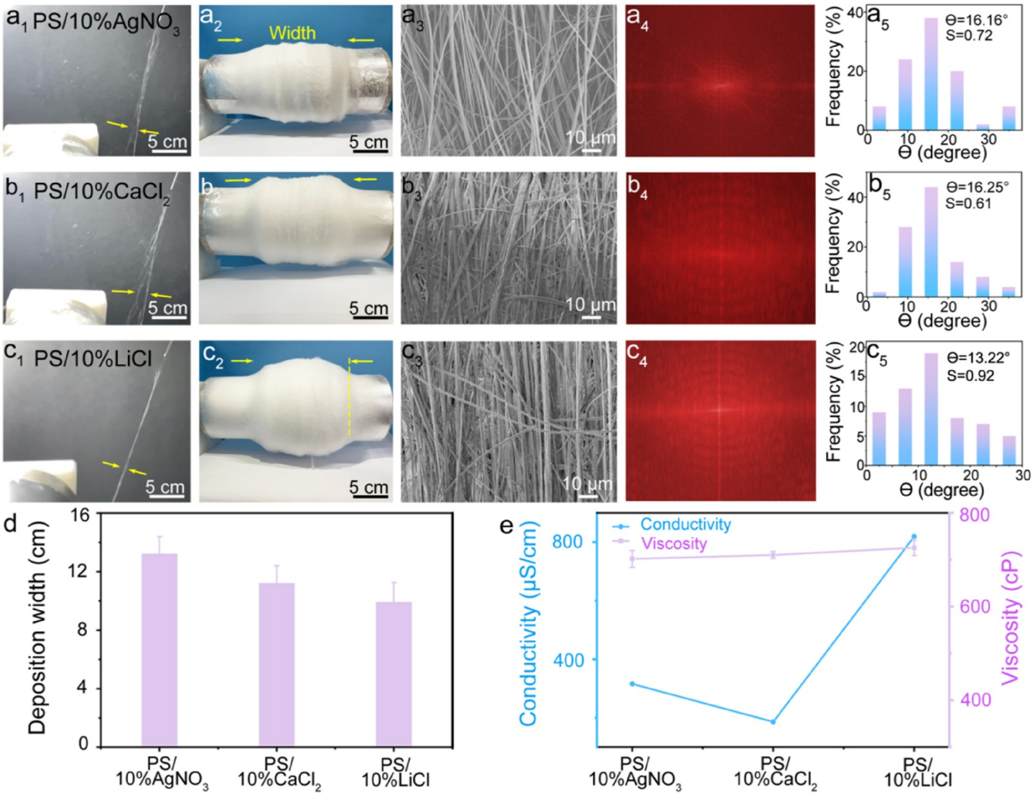

FIGURE 3 | (a_1, a_2) Flying path of the fibre bundle and the resultant PS/10%$AgNO_3$ fibre aerogel. (a_3–a_5) SEM image, FFT result and fibre alignment degree S of the PS/10%$AgNO_3$ fibre aerogel. (b_1, b_2) Flying path of the fibre bundle and the obtained PS/10%$CaCl_2$ fibre aerogel. (b_3–b_5) SEM image, FFT result and fibre alignment degree S of the PS/10%$CaCl_2$ fibre aerogel. (c_1, c_2) Flying path of the fibre bundle and the obtained PS/10%LiCl fibre aerogel. (c_3–c_5) SEM image, FFT result and fibre alignment degree S of the PS/10%LiCl fibre aerogel. (d) Deposition widths of the three kinds of fibre aerogels. (e) Conductivity and viscosity of the spinning solution containing three different kinds of salt.

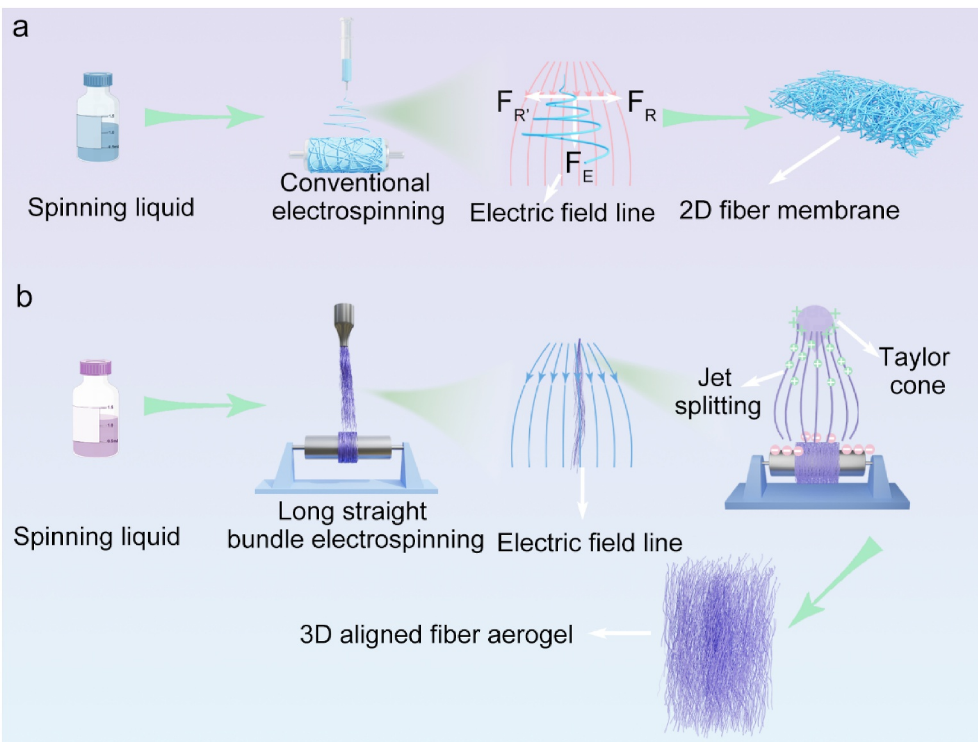

FIGURE 4 | Schematic illustration of the formation mechanism of (a) 2D fibre membrane and (b) bioinspired 3D aligned fibre aerogel.

It was found that salt concentration exerted a profound influence on the formation of the 3D aligned fibre aerogel. This is due to the fact that the electrical conductivity of the spinning solution gradually increased with the addition of salt, and the whipping motion of the fibres would be weakened or even disappeared when the conductivity was high enough. Further studies demonstrated that the addition of different types of salts all resulted in the formation of 3D aligned fibre aerogels. The addition of different types of salts resulted in high electrical conductivities of the spinning liquids, resulting in the weakening of fibre whipping motion.

Thanks to the high conductivity-induced electric field redistribution, long straight fibre bundle electrospinning could be used to prepare 3D fibre aerogel in one step. The whole preparation process was simple and there was no need to further refine the electrospinning setup. It is believed that this one-step scalable method is of great significance for broadening the use of the fibre aerogel.

3.5 | Anisotropic Mechanical Property of the Bioinspired 3D Aligned Fibre Aerogel

The anisotropic tensile mechanical properties of the aligned fibre aerogel were tested in parallel and perpendicular to the direction of aligned fibres, as shown in Figure 5a,b. Figure 5c displayed the tensile strength of the PS fibre membrane and bioinspired aerogel parallel and perpendicular to the direction of fibre alignment, which was 230, 210 and 100 kPa, respectively. The elongation at break of the pure PS fibre membrane was approximately 120%, whereas that of the aerogel in parallel to the fibre alignment direction was 80% and that of the aerogel in perpendicular to fibre alignment direction was only 60% (Figure 5d). As shown in Figure 5e, the Young's modulus of the pure PS fibre membrane and the bioinspired aerogel parallel and perpendicular to the fibre aligned direction was 200, 260 and 150 kPa, respectively. The results indicated that the bioinspired aerogel displayed anisotropic mechanical properties and possessed superior mechanical characteristics in the direction parallel to fibre alignment. When stretched along the direction of fibre alignment, the aerogel was subjected to a more uniform distribution of the total load and was able to withstand higher stresses, resulting in excellent mechanical property. On the contrary, when stretched perpendicular to the direction of fibre alignment, the externally applied stress was difficult to be transferred to the fibres, which ultimately resulted in poor mechanical property [24–26].

3.6 | Potential Application of the Bioinspired 3D Aligned Fibre Aerogel in PM Filtration

As the fibre aerogel showed a unique alignment structure, as a proof of concept, we investigated its potential application in air filtration (Figure 6a). Figure 6b shows the schematic diagram of the anisotropic air filtration performance of the bioinspired aerogel in both parallel to and perpendicular to the fibre alignment direction. As shown in Figure 6c, the filtration efficiencies of the 2D fibre membrane, bioinspired aerogel parallel to the fibre alignment direction and bioinspired aerogel perpendicular to the fibre alignment direction for $PM_{2.5}$ were 97.0%, 99.0% and 97.3%, respectively, whereas the corresponding filtration efficiencies for $PM_{1.0}$ were 97.0%, 98.5% and 97.0%, respectively. Interestingly, their pressure drop was obviously different, which was 79, 21 and 87 Pa, respectively (for $PM_{2.5}$ and $PM_{1.0}$) (Figure 6d). As displayed in Figure 6e, the quality factors of these three filters were 0.048, 0.200 and 0.046 Pa^{-1} for $PM_{2.5}$ filtration and 0.041, 0.170 and 0.040 Pa^{-1} for $PM_{1.0}$ filtration, respectively. The results indicated that, regardless of whether $PM_{2.5}$ or $PM_{1.0}$, the bioinspired aerogel exhibited the enhanced air filtration, reduced pressure drop and superior quality factor in the direction parallel to fibre alignment. It was also found that the filtration efficiency and pressure drop of the bioinspired aerogel did not change significantly after 180 min of filtration, as shown in Figure 6f.

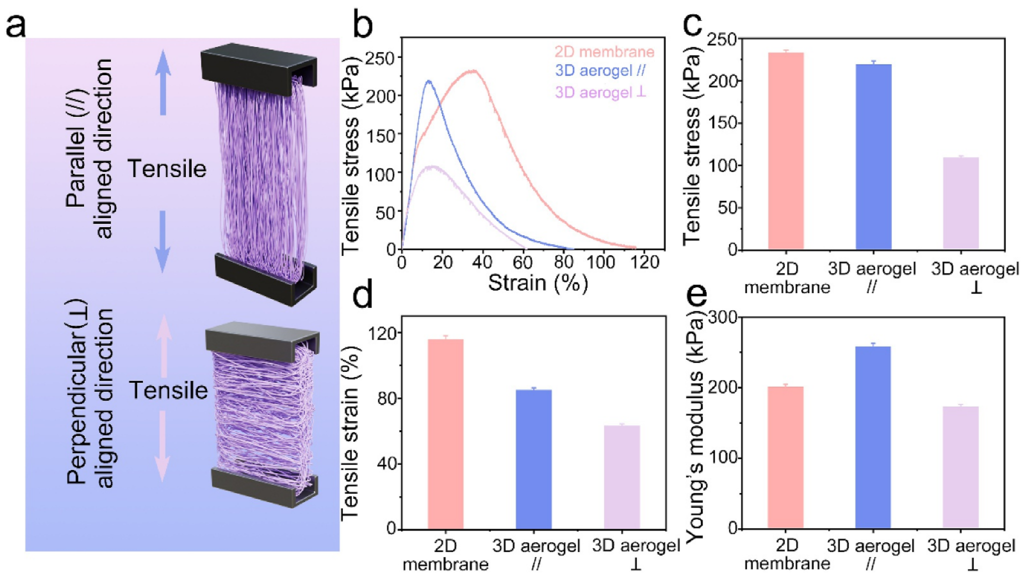

FIGURE 5 | (a) Schematic illustration of anisotropic tensile testing. (b) Stress–strain curves, (c) tensile strength, (d) elongation at break, (e) Young's modulus of the bioinspired 3D aligned fibre aerogel in the direction parallel to and perpendicular to fibre alignment.

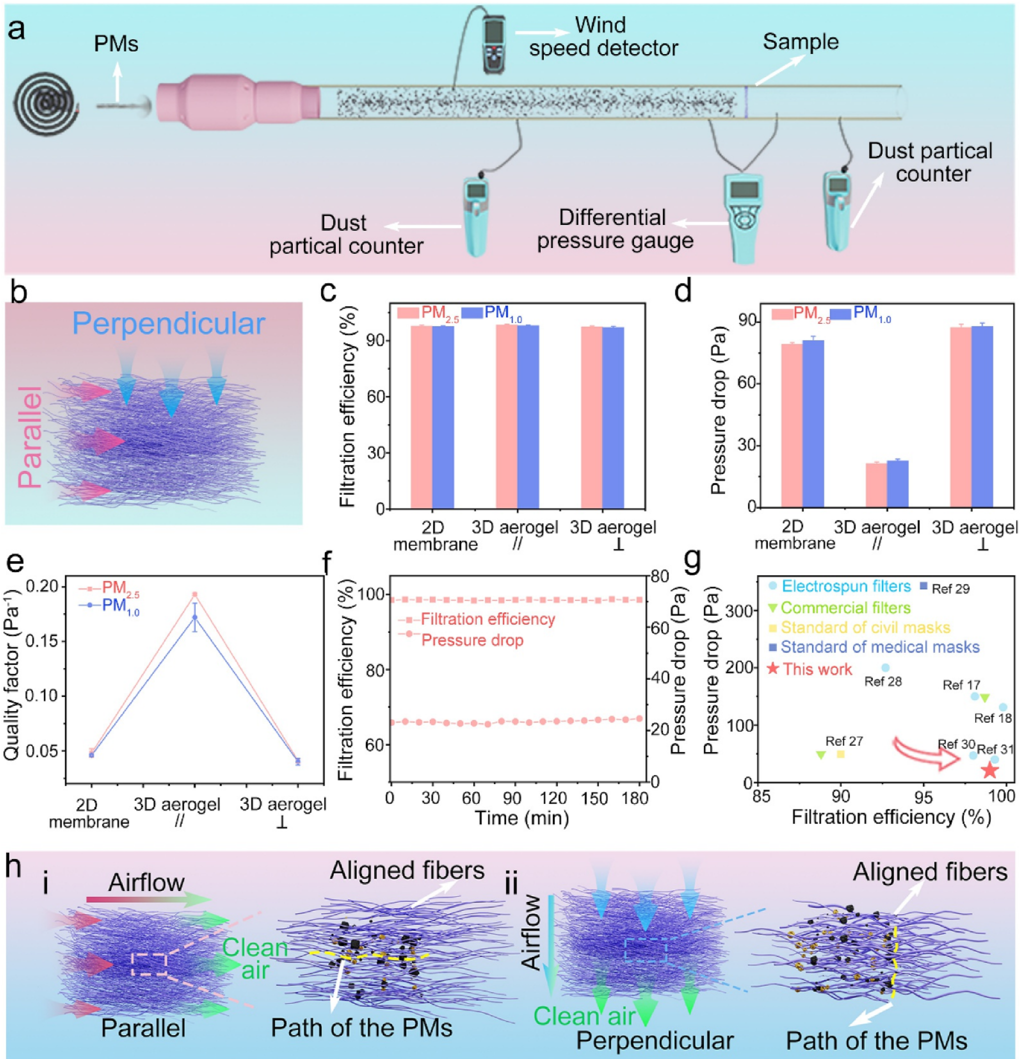

FIGURE 6 | Schematic diagram of (a) air filtration device and (b) anisotropic filtration performance test. (c) Filtration efficiency, (d) pressure drop, (e) quality factor of fibre membrane and aerogel in perpendicular to and parallel to fibre alignment directions for $PM_{2.5}$ and $PM_{1.0}$. (f) Long-term filtration performance of the bioinspired aerogel. (g) Comparison of the filtration performance of the bioinspired aligned aerogel with other air filters, commercial filters and industry standards [17, 18, 27–31]. (h) Schematic illustration of the anisotropic filtration performance mechanism of the bioinspired aligned aerogel.

The filtration performance of the fibre aerogel prepared in this study meets the requirements of relevant standards (GB 19083–2010 and T/CNTAC 55-2020). The filtration performance of the bioinspired aerogel was further compared with that of the commercially available fibre filters and the reported fibre filtration materials, as shown in Figure 6g and Table 1 [17, 18, 27–31]. The results indicated that the filtration efficiency, especially the pressure drop, of the bioinspired aerogel was superior to that of the commercial products and the reported air filters.

We carefully investigated the mechanism of the anisotropic filtration performance of the bioinspired aerogel (Figure 6h). When filtered parallel to the direction of fibre alignment, particles slid radially along the surface of the aligned fibres and were eventually deposited on the fibre surface due to gravity and diffusion, resulting in high filtration efficiency. When filtered along the direction perpendicular to fibre alignment, particles were physically intercepted by impacting with the intricate fibre network, ultimately leading to high filtration efficiency [32]. It was worth noting that the bioinspired fibre aerogel in the direction parallel to fibre alignment showed a particularly low pressure drop. The low pressure drop was resulted from the synergistic coupling of anisotropic permeability and slip flow effect. In contrast to isotropic random fibre networks, our 3D aligned fibre architecture established well-defined, low-resistance flow channels oriented parallel to the fibre axis. This structural anisotropy substantially reduced flow path tortuosity. Furthermore, the slip flow effect also played a critical role since the flow direction coincided precisely with the local fibre orientation. Due to the ultrahigh porosity and the more pronounced slip flow effect between airflow and aligned fibres, collisions of particles with fibres were reduced, resulting in a lower pressure during the filtration process and lower respiratory resistance [17, 33–35].

TABLE 1 | Comparison of the filtration performance of bioinspired 3D aligned fibre aerogel, industry standards, reported filters and commercial filters.

Sample	Filtration efficiency (%)	Pressure drop (Pa)	QF (Pa^{-1})	Reference
Bioinspired aligned fibre aerogel	99.0	21	0.200	This work
Civil protective masks T/CNTAC 55-2020	$\geq$ 90.0	$\leq$ 49	—	[27]
Technical requirements of medical protective masks GB 19083-2020	Level 1 $\geq$ 95.0 Level 2 $\geq$ 99.0 Level 3 $\geq$ 99.9	$\leq$ 343	—	[29]
Reported 3D aerogels	92.7	200	0.013	[28]
	98.0	47	0.083	[30]
	98.1	150	0.026	[17]
	99.3	40	0.124	[31]
	99.8	131	0.047	[18]
Commercial musk	88.7	49	0.044	—
KN95 musk	98.9	150	0.031	—

4 | Conclusions

In summary, we proposed a simple and versatile approach to fabricate the bioinspired 3D aligned fibre aerogel. The key of this method was to control the formation fibre bundles and bundle motion path by manipulating the electrical lines distribution. By doing so, the whipping motion of the fibres was eliminated, and the fibre bundles could undergo a straight motion and freely wrap onto the collector to form the 3D aligned fibre aerogel. This novel method was extremely simple, which did not need any complicated setup. Besides, this method was capable of fabricating the aligned fibre aerogel with a large area in one step. Due to these merits, a polymer aerogel with high fibre alignment degree and thickness of 2.8 cm was prepared. As a proof of concept, this aerogel was utilised in air filtration performance; the bioinspired aerogel exhibited superior air filtration performance in the direction parallel to fibre alignment. The filtration efficiencies for $PM_{2.5}$ and $PM_{1.0}$ were 99.0% and 98.5%, respectively, whereas the pressure drop was only 21 Pa. The air filtration performance of our aerogel was significantly better than that of the commercialised products and reported air filtration materials. This novel preparation strategy may provide a reference for the preparation of 3D fibre aerogels with aligned structures for the applications of oil–water separation, tissue regeneration, desalination and other related fields.

Funding

This work was supported by the Natural Science Basic Research Plan in Shaanxi Province (2024JC-YBMS-399).

Conflicts of Interest

The authors declare no conflicts of interest.

Data Availability Statement

The data that support the findings of this study are available from the corresponding author upon reasonable request.

References

1. H. Maleki and N. Hüsing, “Current Status, Opportunities and Challenges in Catalytic and Photocatalytic Applications of Aerogels: Environmental Protection Aspects,” *Applied Catalysis B: Environmental* 221 (2018): 530–555, https://doi.org/10.1016/j.apcatb.2017.08.012.

2. N. Lavoine and L. Bergström, “Nanocellulose-Based Foams and Aerogels: Processing, Properties, and Applications,” *Journal of Materials Chemistry A* 5, no. 31 (2017): 16105–16117, https://doi.org/10.1039/c7ta02807e.

3. G. Zhao, L. Shi, G. Yang, X. Zhuang, and B. Cheng, “3D Fibrous Aerogels From 1D Polymer Nanofibers for Energy and Environmental Applications,” *Journal of Materials Chemistry A* 11, no. 2 (2023): 512–547, https://doi.org/10.1039/d2ta05984c.

4. M. Dilamian, M. Joghataei, Z. Ashrafi, C. Bohr, S. Mathur, and H. Maleki, “From 1D Electrospun Nanofibers to Advanced Multifunctional Fibrous 3D Aerogels,” *Applied Materials Today* 22 (2021): 100964, https://doi.org/10.1016/j.apmt.2021.100964.

5. S. A. Hashemi, A. Ghaffarkhah, M. Goodarzi, et al., “Liquid-Templating Aerogels,” *Advanced Materials* 35, no. 42 (2023): 2302826, https://doi.org/10.1002/adma.202302826.

6. Y. Chen, Z. Zhang, Y. Lai, et al., “Self-Assembly of 3D Neat Porous Carbon Aerogels With NaCl as Template and Flux for Sodium-Ion Batteries,” *Journal of Power Sources* 359 (2017): 529–538, https://doi.org/10.1016/j.jpowsour.2017.05.066.

7. C. Liu, M.-C. Li, X. Liu, G. Zhou, C. Liu, and C. Mei, “3D Printing of Customized Lignocellulose Nanofibril Aerogels for Efficient Thermal Insulation,” *Additive Manufacturing* 78 (2023): 103841, https://doi.org/10.1016/j.addma.2023.103841.

8. L. Qiao, N. Li, L. Luo, et al., “Design of Monolithic Closed-Cell Polymer Foams via Controlled Gas-Foaming for High-Performance Solar-Driven Interfacial Evaporation,” *Journal of Materials Chemistry A* 9, no. 15 (2021): 9692–9705, https://doi.org/10.1039/d1ta01032h.

9. C.-W. Lou, X. Zhou, X. Liao, et al., “Sustainable Cellulose-based Aerogels Fabricated by Directional Freeze-Drying as Excellent Sound-Absorption Materials,” *Journal of Materials Science* 56, no. 33 (2021): 18762–18774, https://doi.org/10.1007/s10853-021-06498-6.

10. L. Cao, X. Yu, X. Yin, Y. Si, J. Yu, and B. Ding, “Hierarchically Maze-Like Structured Nanofiber Aerogels for Effective Low-Frequency Sound Absorption,” *Journal of Colloid and Interface Science* 597 (2021): 21–28, https://doi.org/10.1016/j.jcis.2021.03.172.

11. P. Zhu, Z. Yu, H. Sun, et al., "3D Printed Cellulose Nanofiber Aerogel Scaffold With Hierarchical Porous Structures for Fast Solar-Driven Atmospheric Water Harvesting," *Advanced Materials* 36, no. 1 (2024): 2306653, https://doi.org/10.1002/adma.202306653.

12. X. Jin, A. Al-Qatatsheh, K. Subhani, and N. V. Salim, "Biomimetic and Flexible 3D Carbon Nanofiber Networks With Fire-Resistant and High Oil-Sorption Capabilities," *Chemical Engineering Journal* 412 (2021): 128635, https://doi.org/10.1016/j.cej.2021.128635.

13. Y. Chen, M. Shafiq, M. Liu, Y. Morsi, and X. Mo, "Advanced Fabrication for Electrospun Three-Dimensional Nanofiber Aerogels and Scaffolds," *Bioactive Materials* 5, no. 4 (2020): 963–979, https://doi.org/10.1016/j.bioactmat.2020.06.023.

14. Z. Yuan, B. Zhou, K. Yuan, et al., "High-Aligned Oppositely-Charged Nanocellulose/MXene Aerogel Membranes Through Synergy of Directional Freeze-Casting and Structural Densification for Osmotic-Energy Harvesting," *Nano Energy* 124 (2024): 109450, https://doi.org/10.1016/j.nanoen.2024.109450.

15. V. Kuzmin, K. Safiullin, A. Stanislavovas, E. Baibekov, and M. Tagirov, "Diffusion Anisotropy of Gaseous Helium-3 in Ordered Aerogels at Low Temperatures," *Journal of Physical Chemistry B* 127, no. 6 (2023): 1459–1470, https://doi.org/10.1021/acs.jpcb.2c08251.

16. S. Dong, B. Maciejewska, R. Millar, and N. Grobert, "3D Electrospinning of Al_2O_3/ZrO_2 Fibrous Aerogels for Multipurpose Thermal Insulation," *Advanced Composites and Hybrid Material* 6, no. 5 (2023): 186, https://doi.org/10.1007/s42114-023-00760-y.

17. M. Li, L. Su, H. Wang, et al., "Stretchable and Compressible Si_3N_4 Nanofiber Sponge With Aligned Microstructure for Highly Efficient Particulate Matter Filtration Under High-Velocity Airflow," *Small* 17, no. 26 (2021): 2100556, https://doi.org/10.1002/smll.202100556.

18. M. Li, L. Xiao, P. Guo, et al., "Resilient and Antipuncturing Si_3N_4 Nanofiber Sponge," *Nano Letters* 23, no. 4 (2023): 1289–1297, https://doi.org/10.1021/acs.nanolett.2c04475.

19. Z. Zhu, S. Fu, and L. A. Lucia, "A Fiber-Aligned Thermal-Managed Wood-Based Superhydrophobic Aerogel for Efficient Oil Recovery," *ACS Sustainable Chemistry & Engineering* 7, no. 19 (2019): 16428–16439, https://doi.org/10.1021/acssuschemeng.9b03544.

20. W. Panatdasirisuk, Z. Liao, T. Vongsetskul, and S. Yang, "Separation of Oil-in-Water Emulsions Using Hydrophilic Electrospun Membranes With Anisotropic Pores," *Langmuir* 33, no. 23 (2017): 5872–5878, https://doi.org/10.1021/acs.langmuir.7b01138.

21. C. Vaquette, C. Kahn, C. Frochot, et al., "Aligned poly(L-lactic-co-e-caprolactone) Electrospun Microfibers and Knitted Structure: A Novel Composite Scaffold for Ligament Tissue Engineering," *Journal of Biomedical Materials Research, Part A* 94A, no. 4 (2010): 1270–1282, https://doi.org/10.1002/jbm.a.32801.

22. X. Cheng, Y.-T. Liu, Y. Si, J. Yu, and B. Ding, "Direct Synthesis of Highly Stretchable Ceramic Nanofibrous Aerogels via 3D Reaction Electrospinning," *Nature Communications* 13, no. 1 (2022): 2637, https://doi.org/10.1038/s41467-022-30435-z.

23. D. Ji, Y. Lin, X. Guo, et al., "Electrospinning of Nanofibres," *Nature Reviews Methods Primers* 4 (2024): 1, https://doi.org/10.1038/s43586-023-00278-z.

24. Y. Pu, X. Yang, Y. Zhang, et al., "Fabrication and Characterization of Highly Oriented Composite Nanofibers With Excellent Mechanical Strength and Thermal Stability," *Macromolecular Materials and Engineering* 305, no. 3 (2020): 1900691, https://doi.org/10.1002/mame.201900691.

25. M. Ahmadi Bonakdar, X. Y. Chen, A. A. Sarbanha, and D. Rodrigue, "Polybutylene Succinate Auxetic Membrane Produced by Solution Electrospinning," *Advanced Engineering Materials* 25, no. 21 (2023): 2300699, https://doi.org/10.1002/adem.202300699.

26. S. Wang, T. Li, C. Chen, et al., "Transparent, Anisotropic Biofilm With Aligned Bacterial Cellulose Nanofibers," *Advanced Functional Materials* 28, no. 24 (2018): 1707491, https://doi.org/10.1002/adfm.201707491.

27. J. Wang, S. Liu, X. Yan, et al., "Biodegradable and Reusable Cellulose-Based Nanofiber Membrane Preparation for Mask Filter by Electrospinning," *Membranes* 12, no. 1 (2022): 23, https://doi.org/10.3390/membranes12010023.

28. Y. Shen, J. Xing, S. Sun, et al., "Biomimetic Strategy to Prepare Thermostable Polyimide Micro/Nanofiber Assembled Aerogels for Airborne Particles Filtration," *Journal of Environmental Sciences* 10, no. 6 (2022): 108923, https://doi.org/10.1016/j.jece.2022.108923.

29. H. Chan, K. Fang, T. Li, L. Zhang, Q. Zheng, and Y. Liang, "Green Preparation of Water-Stable Coptidis-Dyeing Composite Nanofiber Filters With Ultraviolet Shielding and Antibacterial Activity and Biodegradability," *Separation and Purification Technology* 336 (2024): 126289, https://doi.org/10.1016/j.seppur.2024.126289.

30. Y. Hua, Y. Li, Z. Ji, et al., "Dual-Bionic, Fluffy, and Flame Resistant Polyamide-Imide Ultrafine Fibers for High-Temperature Air Filtration," *Chemical Engineering Journal* 452 (2023): 139168, https://doi.org/10.1016/j.cej.2022.139168.

31. T. Liu, C. Cai, R. Ma, et al., "Super-Hydrophobic Cellulose Nanofiber Air Filter With Highly Efficient Filtration and Humidity Resistance," *ACS Applied Materials and Interfaces* 13, no. 20 (2021): 24032–24041, https://doi.org/10.1021/acsami.1c04258.

32. H. Liu, Y. Zhu, C. Zhang, Y. Zhou, and D.-G. Yu, "Electrospun Nanofiber as Building Blocks for High-Performance Air Filter: A Review," *Nano Today* 55 (2024): 102161, https://doi.org/10.1016/j.nantod.2024.102161.

33. Y. Hu, R. Ni, Q. Lu, et al., "Functionalized Multi-Effect Air Filters With Bimodal Fibrous Structure Prepared by Direction Growth of Keratin Nanofibers," *Separation and Purification Technology* 302 (2022): 122070, https://doi.org/10.1016/j.seppur.2022.122070.

34. S. Song, W. Ham, and S.-E. Ahn, "Recyclable Aligned Carbon Nanotube-Sheet-Based Particulate Air Filter With High Filtration Efficiency and Low Pressure Drop," *Current Applied Physics* 36 (2022): 131–136, https://doi.org/10.1016/j.cap.2022.01.014.

35. J. Bae, J. Lee, W.-T. Hwang, et al., "Advancing Breathability of Respiratory Nanofilter by Optimizing Pore Structure and Alignment in Nanofiber Networks," *ACS Nano* 18, no. 2 (2024): 1371–1380, https://doi.org/10.1021/acsnano.3c06060.